European Journal of Pharmaceutics and Biopharmaceutics 142 (2019) 518–530

Contents lists available at ScienceDirect

European Journal of Pharmaceutics and Biopharmaceutics

journal homepage: www.elsevier.com/locate/ejpb

Research paper

Synthesis and characterization of acetyl curcumin-loaded core/shell liposome nanoparticles via an electrospray process for drug delivery, and theranostic applications

Ankireddy Seshadri Reddy[a,1], Buddolla Anantha Lakshmi[b,1], Sanghyo Kim[b], Jongsung Kim[a,*]

[a] Department of Chemical & Biological Engineering, Gachon University, Sungnam 13120, Republic of Korea
[b] Department of Bionanotechnology, Gachon University, San 65, Bokjeong-Dong, Sujeong-Gu, Seongnam-Si, Gyeonggi-Do 461-701, Republic of Korea

ARTICLE INFO

Keywords:
Core/shell liposome nanoparticles
Curcumin
Acetyl curcumin
Drug delivery
Screening of anticancer activity
Kinetic models

ABSTRACT

Despite substantial advancements in divergent drug delivery systems (DDS), there is still room for novel and innovative nanoparticle-mediated drug delivery methodologies such as core/shell liposomes to deliver drugs in a kinetically controlled manner into the active site without any side effects. Herein, ((1E,6E)-3,5-dioxohepta-1,6-diene-1,7-diyl) bis (2-methoxy-4,1-phenylene) diacetate acetyl curcumin (AC)-loaded poly(lactic-co-glycolic acid) (PLGA) core/shell liposome nanoparticles (ACPCSLNPs) were prepared using an electron spray method under an applied electric field, which facilitated the uniform formation of nano-sized liposome nanoparticles (LNPs). Then, kinetically controlled and sustained drug release profiles were investigated using the as-prepared ACPCSLNPs. Moreover, the inner polymeric core could not only induce the generation of electrostatic interactions between the polymer and drug molecules but could also affect the prominent repulsions between the polar head groups of lipids and the nonpolar drug molecules. As a result, the sustained maximum release of the drug molecules (~48.5%) into the system was observed over a long period (~4 days). Furthermore, cell cytotoxicity studies were conducted in a human cervical cancer cell line (HeLa) and a healthy human dermal fibroblast cell line (HDFa) by employing all AC loaded LNPs along with free drugs. Multicolor cell imaging was also observed in HeLa cells using ACPCSLNPs. Notably, more curcumin was released from the ACPCSLNPs than AC due to the presence of polar group attractions and polar-polar interactions between the lipid head groups and curcumin since curcumin is more soluble than AC in aqueous medium. In addition, the predictions of the release kinetic patterns were also investigated thoroughly using the exponential-based Korsmeyer-Peppas (K-P) and Higuchi models for drug-loaded LNPs and PLGA NPs, respectively.

1. Introduction

Physicochemical parameters such as solubility, pH, and diffusivity always play vital roles in the use of advanced and novel DDS for theranostic applications in any biological system [1]. However, solubility and diffusion are essential and critical barriers for the transportation of all kinds of drug molecules into the corresponding site of action since most of the active drug molecules are amphiphilic in nature. As a result, it is quite difficult to distribute polar and nonpolar drug molecules into their corresponding environments to achieve significant responses and efficacies [2,3]. To overcome the aforementioned complications, conventional DDS were initially evolved for the delivery of essential drugs and other important biological molecules to the cells of interest [4]. However, these conventional DDS are not recommended for clinical applications that require a long period of release due to the remarkable adverse side effects that can occur by the distribution of

Abbreviations: Cur, Curcumin; AC, Acetyl Curcumin; LNPs, Liposome nanoparticles; PCSLNPs, PLGA polymer loaded core/shell liposome nanoparticles; CLNPs, Curcumin loaded liposome nanoparticles; AC-LNPs, Acetyl Curcumin loaded liposome nanoparticles; CPCSLNPs, Curcumin loaded PLGA core/shell liposome nanoparticles; ACPCSLNPs, Acetyl Curcumin loaded PLGA core/shell liposome nanoparticles; PLGA, Poly(lactic-co-glycolic acid); PLGA-NPs, Poly(lactic-co-glycolic acid) nanoparticles; CPLGA-NPs, Curcumin loaded poly(lactic-co-glycolic acid) nanoparticles; ACPLGA-NPs, Acetyl Curcumin loaded poly(lactic-co-glycolic acid) nanoparticles; IMHB, Inter molecular hydrogen bonding; H-bonding, hydrogen bonding; DDS, Drug delivery systems; MTT, (3-(4,5-Dimethylthiazol-2-yl)-2,5-Diphenyltetrazolium Bromide); DMEM, Dulbecco's Modified Eagle Medium

* Corresponding author.
E-mail address: jongkim@gachon.ac.kr (J. Kim).
[1] A.S.R., and B.A.L. contributed equally to this work.

https://doi.org/10.1016/j.ejpb.2019.07.024
Received 29 March 2019; Received in revised form 17 July 2019; Accepted 27 July 2019
Available online 28 July 2019
0939-6411/ © 2019 Elsevier B.V. All rights reserved.

unintended cargoes beyond their design [5]. Subsequently, divergent DDS using polymeric nanoparticles [6], polymers [4,7], polymer-mediated nanofibers [8], carbon-based particles (e.g., graphene oxide and carbon nanotubes) [9,10], magnetic nanoparticles [11], silica [12], gold nanoparticles [13] and metal organic frameworks (MOFs) [14] have made tremendous progress as theranostic agents. However, these DDS also suffer from considerable drawbacks due to several reasons at the pharmacokinetic level including unfavorable cellular toxicity issues that are based on the presence of toxic entities and nondegradable toxic polymers [15].

In response to this major global health concern, liposome nanoparticles exhibit outstanding performance over conventional and toxic nanoparticle-mediated DDS for theranostic applications because not only are the liposomes naturally occurring phospholipids but the created system also mimics the original cell environment since it resembles the plasma membrane lipid bilayer [4]. In addition, other biomolecules, such as proteins and cholesterol, are also embedded between the lipid bilayer matrix. Eventually, this system can also enable a clear path for the distribution of polar and nonpolar molecules across the membrane [16]. More importantly, the LNPs are 3D spheres with polar carboxyl head groups oriented outside, and the nonpolar fatty acid tails are merged between two layers in an aqueous medium; this configuration not only creates an additional means of active and passive distribution for the essential metal ions and biomolecules but also makes the kinetically sustained release of drug molecules feasible via existing hydrogen bonding or electrostatic interactions. On the basis of these ideal biocompatible pharmacokinetic properties, innumerable efforts have been continuously undertaken for diverse applications such as treatment for anticancer, neurological, and cardiovascular disorders [17–21]. As per the medical reports, some drug-loaded liposome nanoparticles have already been evaluated as liposomal drug formulations [22,23], and some drug-loaded liposome nanoparticles are under investigation in clinical trials [24,25]. Furthermore, remarkable progress has also been made to develop DDS that can work for long periods using core/shell liposome nanoparticles. In particular, this system should not only have an inner core that can release a minimal amount of drug slowly into the system but should also allow the nanoparticle to withstand various physiological conditions to perform more effectively than LNPs.

The core/shell DDS with polymeric materials as an inner core has led to a paradigm switch in a safe and convenient approach for the delivery of drug molecules at active site. To date, a variety of nanoparticle, polymeric, and hydrogel-oriented inner cores have been employed, and significant progress has also been made for different drug delivery applications [26–29]. However, the inner core from biodegradable polymeric nanoparticle has been gaining greater attention because of having several superior qualities such as biocompatibility, flexibility, excellent stability with efficient drug loading capability, a combination of polar and non-polar functionalities to mimic the bio-environments. As a result, there is an opportunity to create multiphase environments not only in the outer lipid bilayer but also in the inner core eventually to release drug molecules at an active site with sustainable and kinetically controlled manner for a prolonged period without considerable adverse effects. Among the list of various biodegradable polymers, PLGA is a co-polymer, which has been prepared from the combination of natural lactic and glycolic acids. Interestingly, the majority of the formulations have been focused on PLGA as a polymeric inner core because of having the essential functional groups for both hydrophilic and hydrophobic drugs could hold into the matrix via hydrogen bonding, and van der Waals forces than the other biodegradable polymers. On the other wards, chitosan, cellulose, methyl cellulose polymers have the more polar functional groups, which can be generating the hydrophilic core, which eventually more likely favorable for the polar drug molecules than nonpolar drugs [30]. Based on the aforementioned distinct phases in the core/shell PLGA liposome nanoparticles, although the absence of polar functional groups in AC can have an excellent capability to link with the PLGA core via van der Waals interactions and along with hydrophobic nature. Thus, the developed core/shell PLGA nanocarrier system can allow the AC drug molecules into the stream kinetically in slow manner with desirable amount. Several reports are available so far on drug loaded PLGA core/shell liposome nanoparticles as an ideal DDS for numerous theranostic applications. However, drug loaded LNPs and PCSLNPs preparation using electrospray method, desirable amounts of sustain drug delivery methodologies with kinetic studies in different physiological conditions along with theranostic applications as innovative insights that have been investigated thoroughly than other published reports [31–45].

In the past several decades, cancer has been one of the major serious health concerns across the globe. Despite the existence of rapid technology and potential treatment methods, molecular-level mechanisms for cancer have yet to be established [46]. According to medical reports, considerable prevention measures have been observed using natural products and their derivatives for constructive treatments with negligible side effects because of their biocompatibility [47]. Among these natural products, curcumin is a bright yellow flavonoid compound that is a major constituent in the root of curcuminoid turmeric (Curcuma longa) and belongs to the Zingiberaceae family. Curcumin has outstanding medicinal value along with anticancer, anti-oxidant, anti-inflammatory and anti-viral properties and has been widely used for ancient medicines [48]. Interestingly, it is well known that curcumin is sparingly soluble in aqueous mediums and highly soluble in organic solvents, which leads to its low bioavailability [49]. Fluorescence imaging (bio-imaging) for cancer has various advantages such as excellent temporal resolution, cost-effectiveness, and safety, all of which have been reported in the previous literature [50]. Feng. T et al. already reported liposomal curcumin formulations that demonstrated excellent drug delivery and anticancer effects in cancer cells [51].

The basic mechanism for the electrospray system is that synthesis of nanoparticles in a chamber contain a precursor solution with low surface charge density under the applied high electric field. During this process solvent evaporation will occur before Rayleigh limit reach, which eventually led to the formation of shrinking of a droplet and followed by the coulomb fission occurs. As a result, the particle size distribution will change and it causes the disintegration of particles to form nanoparticles when coulomb fission is generated. The solvent density, type, and gauge of needle and amount of applied electric field could influence the formation of desired nanoparticles with size and shape [52]. In general, different solvents, surfactants, and reducing agents have been employing for the preparation of core/shell nanoparticles. Furthermore, the thin layer evaporation technique, and emulsification, prerelease, nanoprecipitation/solvent displacement, and microfluidic approaches are available for the rapid preparation of these nanoparticles from various lipid sources. However, several drawbacks were also observed when using these approaches, including the need for different drastic temperature conditions, less drug loading into the nanoparticle matrix and less stability of the nanoparticles, since the particle preparation occurred in various kinds of solvent ratios. However, without using those chemicals, and multistep synthetic procedures, electrospray technique can have the ability to prepare nanoparticles with desired size, shape, proper loading of drug molecules into the spear, and bioactive ingredients immobilization [53]. Thus, we have attempted an electrospray technique under an applied electric field for the synthesis of all LNPs and PLGA NPs to overcome these problems [54]. In this report, AC was prepared using (1E,6E)-1,7-bis(4-hydroxy-3-methoxyphenyl) hepta-1,6-diene-3,5-dione (curcumin) as a precursor with acetic anhydride in the presence of an acidic medium. A prepared drug was employed for the drug-loaded liposome nanoparticle preparation in the presence and absence of a core. Then, the sustained drug release profiles were examined using the as-prepared ACPCSLNPs along with curcumin-loaded PLGA core/shell liposome nanoparticles (CPCSLNPs), AC-loaded liposome nanoparticles (ACLNPs), and curcumin-loaded liposome nanoparticles (CLNPs). In addition, the as-

prepared AC, ACLNPs and ACPCSLNPs were also employed to investigate their anticancer properties in the HeLa cell line. Finally, the drug release profiles of all LNPs, PCSLNPs and PLGA NPs were thoroughly explored using standard kinetic Higuchi and Korsmeyer-Peppas (K-P) models.

2. Experimental section

2.1. Chemicals & apparatus

L-α-Phosphatidylcholine from soybeans [> 99% (TLC) lyophilized powder], cholesterol, curcumin, acetic anhydride (> 98%), conc. H_2SO_4 (98%), dichloromethane (DCM), poly(lactide-co-glycolide) (PLGA) copolymers (50:50), acetone-d_6, *d*ichloromethane-d_2 (CD_2Cl_2), phosphate-buffered saline (PBS), borate buffer saline (BBS), ethyl acetate and ethanol were purchased from Sigma-Aldrich. Becton Dickinson (BD) Luer-Lok™syringes (5 mL size) and 26 G electrospun needles were obtained from BD, South Korea. The Spectra/Pro® dialysis membrane (MWCO: 500–1000 D) was purchased from Biotech CE Tubing, Spectrum labs, South Korea. A human cervical cancer cell line (HeLa) and a healthy fibroblast cell line (HDFa) were obtained from CEFO Ltd, South Korea. Trypsin-EDTA, Dulbecco's modified eagle's medium (DMEM) and penicillin–streptomycin solution were purchased from Gibco Laboratories, Korea. Fetal bovine serum (FBS) was obtained from Young in Frontier, Korea. The Live/Dead™ viability/cytotoxicity cell staining kit and 3-(4,5-dimethylthiazol-2-yl)-2,5-diphenyltetrazolium bromide (MTT) assay kit were purchased from Thermo Fisher Scientific, USA. All chemicals were analytical grade and used directly without any further modification.

2.2. Instrumentation

The morphological characterizations were performed using scanning electron microscopy (SEM) on a S-4700 with an accelerating voltage of 20 kV from HITACHI, Japan. X-ray photoelectron spectroscopy (XPS) with a Sigma Probe spectrometer (Thermo VG) equipped with an A1-Kα source (15 kV, 100 W, 400 μm) system was employed to measure the complete chemical and elemental analysis. An electrospinning instrument (NanoNC, Co., South Korea) was used for the preparation of all LNPs. The prepared AC structure was confirmed using ^{1}H and ^{13}C NMR analysis, and the spectra were obtained on a Bruker Avance III 500 MHz from Germany. Tetramethylsilane (TMS) as an internal reference, acetone-d_6, and dichloromethane-d_2 (CD_2Cl_2) as a solvent were used to obtain the corresponding NMR spectra. The coupling constants, *J*, were given in Hz, and chemical shifts are represented in δ (ppm units) relative to TMS. The functional group changes in all samples were recorded using Fourier transform infrared (FTIR) spectra on a high-resolution Bruker Vortex 70 FTIR spectrometer. The ultraviolet–visible (UV–vis) spectra of the absorbance change by the released drug and the standard calibration curves of AC and curcumin were recorded using a Varian Cary 100 UV–vis spectrophotometer from Agilent Technologies, South Korea. The ELSZ-2000 series zeta-potential and particle size analyzer were employed for the analysis of the as-prepared LNPs particle sizes in PBS buffer. The NIKON live cell capture system was employed for fluorescence, and live & dead cell imaging.

2.3. General procedure for the synthesis of ((1E,6E)-3,5-dioxohepta-1,6-diene-1,7-diyl) bis (2-methoxy-4,1-phenylene) diacetate

In a systematic procedure, 0.542 mmol (200 mg) (1E,6E)-1,7-bis(4-hydroxy-3-methoxyphenyl) hepta-1,6-diene-3,5-dione (curcumin) was added to a round bottom flask (RBF) containing 5 mL acetic anhydride and 5 mL ethanol, and the reaction mixture was refluxed for 20 min in the presence of an acidic medium (100 μL H_2SO_4 0.001 N). The reaction was monitored by TLC. Meanwhile, the color of curcumin changed significantly from yellow to dark brown if acetylation occurred (Fig. S1). Then, the final desired product settled down at the bottom of the RBF as a deep brown-colored compound after the reaction mixture was immediately cooled in an ice bath. The resulting mixture was filtered with DI water several times to remove unreacted chemicals. Then, the product was purified by column chromatography on silica gel to afford the final product in pure form. The product was a dark brown solid compound that was synthesized with a 92.5% (185 mg) yield. mp: 196–200 °C. ^{1}H NMR (500 MHz, acetone-d_6) δ 7.68 (d, J = 8.8 Hz, 1H), 7.45 (s, 1H), 7.29 (d, J = 8.25 Hz, 1H), 7.1 (d, J = 17.4 Hz, 1H), 6.9 (d, J = 16.7 Hz, 1H), 6.0 (s, 2H), 3.8 (s, 3H), 2.4 (s, 3H) ppm. ^{13}C NMR (500 MHz, acetone-d_6): δ 206.32, 168.97, 152.76, 142.62, 140.7, 134.96, 130.23, 125.39, 122.7, 102.54, 60.09, 56.43, 21.06 ppm.

(1E,6E)-1,7-bis(4-hydroxy-3-methoxyphenyl) hepta-1,6-diene-3,5-dione (curcumin) is a yellow-colored compound. mp: 186.5–188.3 °C. ^{1}H NMR (500 MHz, acetone-d_6) δ 8.22 (s, 2H), 7.5 (d, J = 9.1 Hz, 1H), 7.68 (s, 1H), 7.18 (d, J = 8.25 Hz, 1H), 6.98 (d, J = 18 Hz, 1H), 6.7 (d, J = 16.2 Hz, 1H), 5.97 (s, 2H), 3.92 (s, 3H), ppm. ^{13}C NMR (500 MHz, acetone-d_6): δ 206.32, 184.3, 148.85, 141.12, 131.05, 128.23, 123.96, 122.37, 116.85, 111.60, 56.38, 53.42 ppm.

2.4. Synthesis of core/shell liposome nanoparticles

The drug-loaded core/shell liposome nanoparticles along with neat liposome nanoparticles and PLGA NPs were synthesized via an electrospray system using an electrospinning machine under an applied electric field [36]. In a typical procedure, 100 mg of L-α-phosphatidylcholine and 25 mg cholesterol were mixed in a vial containing 1 mL DCM. For the synthesis of neat LNPs, the addition of PLGA polymers into the final reaction mixture was omitted. To synthesize neat LNPs, 4:1 ratio of L-α-phosphatidylcholine and cholesterol were mixed in 1 mL DCM. On the other wards, 50 mg of PLGA was added to the above solution in order to the synthesis of PCSLNPs. Approximately, 50 mg of PLGA was dissolved in 1 mL of DCM for the synthesis of neat PLGA NPs. Finally, for the preparation of drug-loaded LNPs, PCSLNPs, and PLGA NPs, 8.1 mg of the drug (curcumin or AC) was also mixed into the above solution before being loaded into the syringe. Then, the prepared solution was loaded into the Becton Dickinson (BD) Luer-Lok™ syringes and a 26 G needle was fixed and placed on the pump. An approximately 10 μm distance was maintained between the syringe and the particle collector. Subsequently, the corresponding LNPs were sprayed on the glass container by applying a 15 kV high-voltage electric field at a flow rate of 0.6 mL/h with a pump, as illustrated in Fig. 2, and then the solvents were completely evaporated under N_2 atmosphere. Finally, 20 mL PBS (pH = 7.4) was added to the glass container where the LNPs were collected, and the mixture was stirred vigorously for 20 min and directly used as prepared LNPs for future purposes.

2.5. Study of the in vitro drug release profile

A dialysis tubing system was used for the examination of the *in vitro* drug release profile. Indeed, curcumin is sparingly soluble in aqueous medium due to the presence of longer alkyl chains along with aromatic rings; however, the solubility of AC is reduced by the acetylation on both ends. Thus, AC has an approximately 0.1, 15 and 120 mg/mL solubility in DI water, PBS, and ethanol, respectively, at an ambient temperature. Based on the solubility, the entire experiment was conducted in PBS at 37 ± 0.5 °C, which is almost equal to the physiological body temperature. Approximately 5 mL of the prepared drug-loaded LNPs were placed in a cellulose ester dialysis membrane with 50 mL PBS buffer at 5.2 and 7.4 pH, the membrane ends were tagged with clamps, and the membrane was again placed in a beaker containing 100 mL of the released medium (Fig. 2) under constant stirring at 250 rpm. The standard curve was prepared over specific concentration ranges to estimate the amount of released drug, and the corresponding linear curve, which followed the linear behavior of Beer-Lamberts law, is presented in supporting information Fig. S14. Aliquots

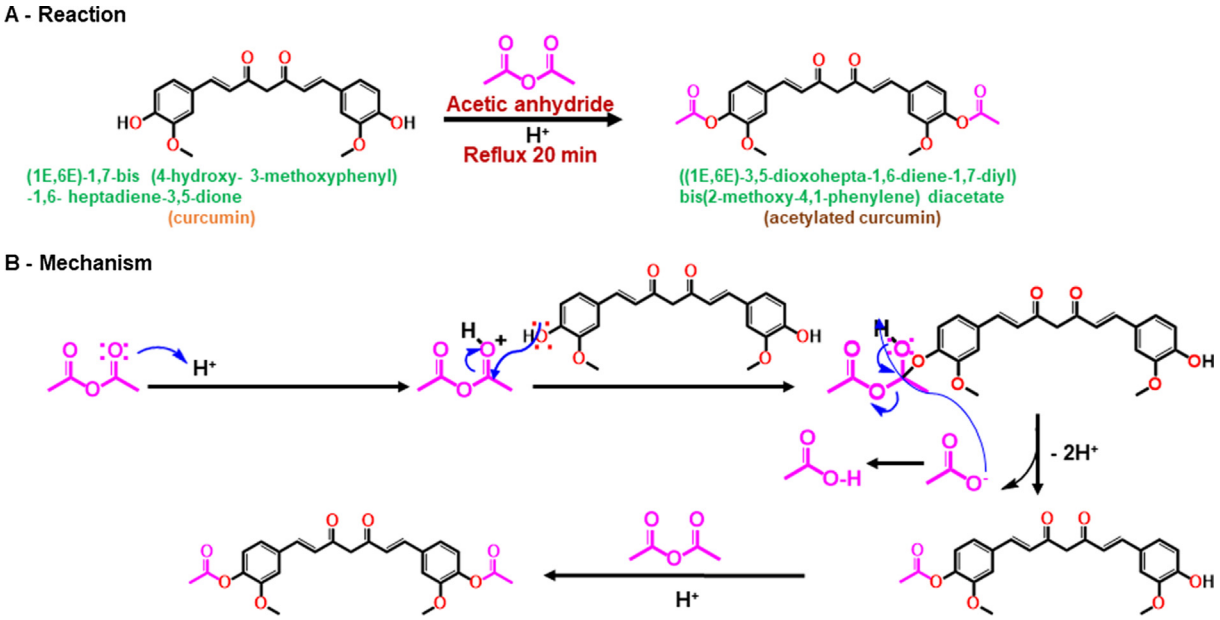

Fig. 1. (A) Schematic representation of the synthesis of AC from curcumin, and (B) detailed reaction mechanism for the formation of the desired product. The complete reaction synthesis has been carried out in ethanol as a solvent.

of the sample were withdrawn periodically from the beaker during the reaction process to examine the drug release kinetics using a UV–vis spectrophotometer. Similarly, the release profiles of other samples such as CPCSLNPs, ACLNPs, and CLNPs along with curcumin, ACPLGA, and CPLGA-NPs were also evaluated under similar experimental conditions.

$$\%\text{of cummulative drug release} = \frac{\text{Amount of drug at time}}{\text{Total drug concentration in the LNPs}} \times 100 \quad (1)$$

2.6. Cell culture

A human cervical cancer cell line (HeLa) and human dermal fibroblast (HDFa) cells were cultured in DMEM supplemented with 10% FBS and 1% penicillin-streptomycin solution and incubated at 37 °C in an incubator with a humidified 5% carbon dioxide environment as per the ATCC guidelines. After reaching 80–90% confluency, the cells were subcultured. In the same manner, HDFa cell lines, which were employed as the healthy control cell line, were also grown by following specified experimental conditions.

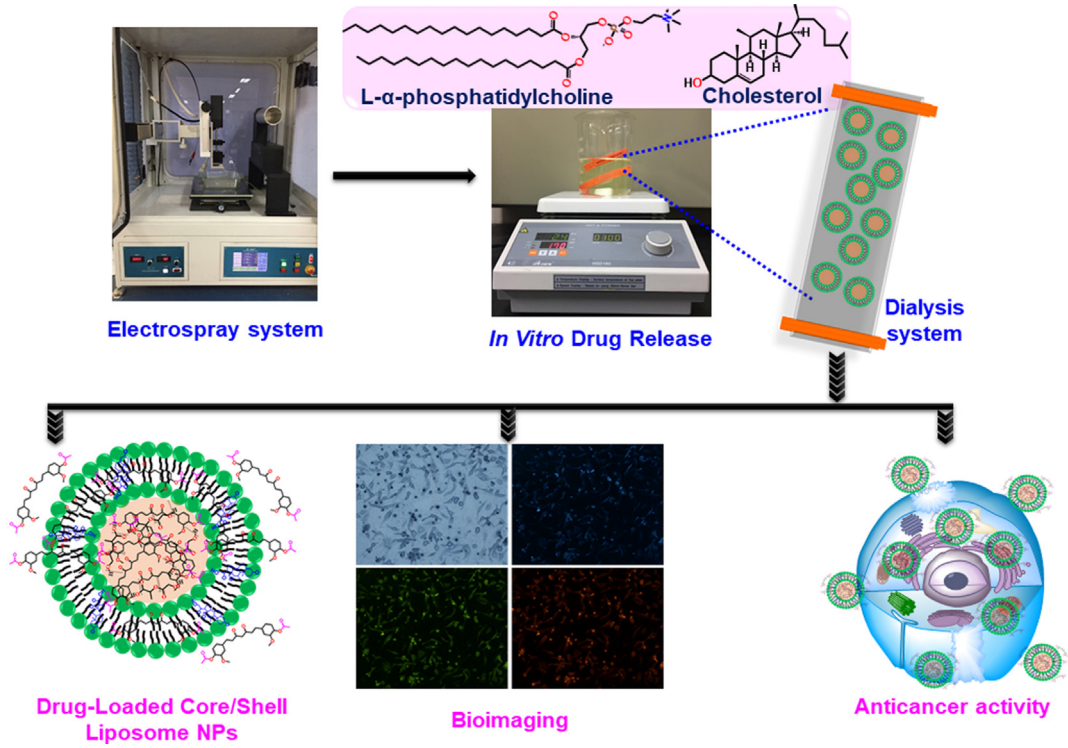

Fig. 2. Schematic illustration of synthesis of liposome nanoparticles using an electrospray system, sustained drug release study, bio-imaging and anticancer screening properties using ACPCSLNPs.

2.7. Cell cytotoxicity studies by MTT assay

An MTT assay was employed to evaluate the cytotoxic effects of the liposomes against the cells. HeLa and HDFa cells were harvested in 96-well plates at a concentration of 1×10^5 cells per mL with the required medium and were incubated for 24 h at 37 °C under 5% CO_2 conditions. After incubation, the culture medium was discarded, and the liposomes (AC, curcumin, ACLNPs (without core) and ACPCSLNPs were added at different concentrations (0, 5, 10, 15, 20, 25, and 30 μM) and incubated for 48 h at 37 °C with 5% CO_2. Then, the solutions were removed and replaced with 50 μL MTT reagent along with 50 μL serum-free medium and allowed to incubate for up to 3 h at 37 °C with 5% CO_2. After incubation, 150 μL of the MTT solvent was added, and the cell viability was evaluated by recording the absorbance at 570 nm [55].

2.8. Cell cytotoxicity studies by live-dead cell staining assay

According to the manufacturer's protocol, a live-dead cell staining kit was used for the assessment of drug-induced changes in cell viability. Cells were grown in a six-well plate by using coverslips and incubated for 24 h at 37 °C with 5% CO_2. Then, the cells were treated with the ACPCSLNPs for distinct time intervals of 0, 12, 24, 36 and 48 h. After the significant time intervals, the coverslips were washed with DPBS, and 150 μL of the freshly prepared live-dead cell staining solution was added to the coverslip surface and incubated in the dark for approximately 30 to 40 min; the stained samples were imaged by fluorescence microscopy. At specific time intervals, both the treated cells and control cells were imaged and differentiated from each other. By using a non-permeable fluorescent dye and a cell-permeable fluorescent dye, dead cells and live cells were stained red and green, respectively. By using the Nikon live cell capture software, the images were processed and acquired.

2.9. Cell imaging studies

Cells were grown on coverslips in a six-well plate in DMEM along with 10% FBS and 1% antibiotics and incubated for 24 h at 37 °C with 5% CO_2. After 24 h of incubation, the medium was discarded, and liposomes (free curcumin, AC and ACPCSLNPs) were added to each well and incubated at 37 °C with 5% CO_2 for 5 h. After incubation, the coverslips were washed with PBS, and the images were obtained by using fluorescence microscopy.

2.10. Statistical analysis

All the results in this paper were stated as the mean of three individualistic experiments (± standard deviation) and the statistical significance was evaluated by employing the student's *t*-test.

3. Results and discussion

3.1. Synthesis

Initially, an active drug (AC) was synthesized from curcumin, and the corresponding mechanism of reaction for the formation of the final product is presented in Fig. 1. As shown in Fig. 1A, acetylation occurred at the 1 and 7 positions at both ends of the curcumin molecule when it was treated with acetic anhydride in the acidic medium under reflux conditions for 20 min. Interestingly, a prominent color change was observed from yellow to dark brown when acetylation occurred. Fig. S1 shows photographic evidence of the product color change before (left image) and after (right image) the reaction. The reaction color changed to a dark brown color within 20 min, which indicated that the reaction was completed successfully. The mechanism of action for the formation of AC from curcumin in the presence of acetic anhydride is depicted in Fig. 1B. As explained in the image, an initial nucleophilic attack occurred on the electrophilic center of the carbonyl group of acetic anhydride from the oxygen atom of a hydroxyl group on curcumin, which eventually led to the formation of a tetrahedral intermediate via a nucleophilic substitution reaction. Soon after, during a nucleophile substitution reaction, an electronegative substituent (acetate ion) that can act as a leaving group was removed from the tetrahedral intermediate once the negative charge on the oxygen atom was reinstated. As a result, the ester group was formed after the acetyl moiety attached to the oxygen atom of curcumin. More interestingly, the other hydroxyl group was also subsequently acetylated after the addition of excess reagent.

In the second step, as-prepared AC was used for the core/shell LNP formulations along with the formulations of the other LNPs and PLGA NPs for comparative studies. The LNP synthesis, sustained drug delivery profile, bio-imaging, and screening for anticancer activity were illustrated in Fig. 2. All LNPs were prepared using an electrospray system with an electrospinning machine under a high electric field. However, using a tiny gauge nozzle (26 G needle) and an applied high-voltage electric field facilitated the formation of uniform nano-sized LNPs and PLGA NPs, which do not require a further process of extrusion like other commercially available NPs [56]. Subsequently, sustained drug release profiles were also thoroughly investigated using a dialysis membrane tubing system by measuring the absorbance of the released drugs via a UV–vis spectrophotometer. The LNPs, drug-loaded LNPs and ACPCSLNPs were immersed in a vial containing PBS solution (Fig. S2) soon after synthesis and subjected to 20 min of vigorous stirring. It can be seen from the figure that bare PCSLNPs virtually resemble a colorless suspension with a uniform particle distribution (Fig. S2(i)). However, Fig. S2(ii) shows that the LNPs were yellow in color due to the addition of AC, which clearly suggests that the drug was successfully loaded inside of the LNP cores. Meanwhile, no considerable yellow color was observed even after loading AC into the PCSLNPs when compared with ACLNPs, which may be due to the fact that the loaded drug completely entered the inner core of the PLGA polymeric matrix (Fig. S2(iii)).

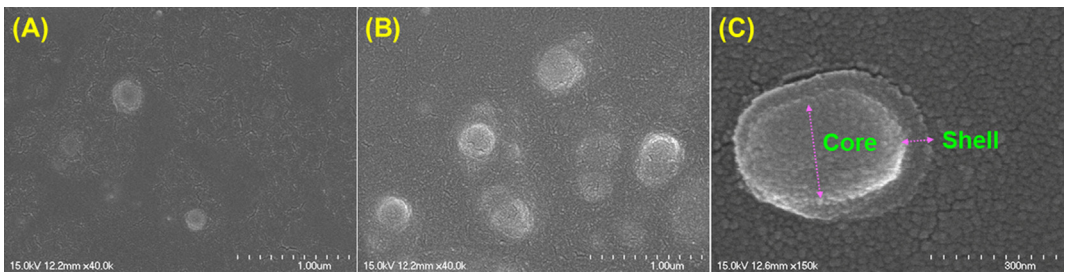

Fig. 3. Scanning electron microscopy images of (A) neat LNPs, (B) ACLNPs, and (C) ACPCSLNPs.

3.2. Morphology

The size and shapes of neat LNPs, ACLNPs, and ACPCSLNPs were examined using a scanning electron microscope, and all LNPs showed spherical shapes with diameters in the nanometer range, as presented in Fig. 3A-C. The transparency of the LNPs and ACLNPs was not clear due to the presence of water or salt buffer [57]. In contrast, neat LNPs (Fig. 3A) and ACLNPs (Fig. 3B) were formed with diameters ranging from ~200–250 and 300–350 nm, respectively, and these results were also consistent with the corresponding hydrodynamic DLS particle size analysis, as shown in Fig. S3A and B. As shown in Fig. 3C, the SEM image of ACPCSLNPs renders the distinct structural features regarding the arrangement of the inner PLGA polymeric core and exterior lipid shell with an average individual diameters ranging from ~380–415 ± 10 and ~30–45 ± 5 nm, respectively, and the complete size of one ACPCSLNP is approximately ~410–450 ± 10 nm [31]. These findings were also in good agreement with the particle sizes that were obtained by using a hydrodynamic DLA particle size analyzer (Fig. S3C). Interestingly, notable size differences were also identified between neat LNPs and core/shell LNPs; based on the size analysis from SEM and DLS, the as-formed bare LNPs, ACLNPs and ACPCSLNPs may be classified as large unilamellar vehicles (LUVs) [58]. In addition, due to the formation of the inner core, one of the possible considerations for the size increase of ACPCSLNPs is the formation of a multi-lipid layer. Fig. S4 illustrates the morphological changes of pure PLGA NPs and AC-loaded PLGA NPs. The figure shows that the randomly oriented pure PLGA NPs have smooth surfaces with an average NP diameter of 350 ± 50 nm (Fig. S4A), while the AC-loaded PLGA NPs have rough surfaces with an average NP diameter of 650 ± 50 (Fig. S4B). The figure also shows that the diameter of the prepared NPs increased after loading AC into the PLGA NP matrix along with the significant appearance of surface roughness. In addition, the SEM analysis showed that NPs with unique and uniform sizes were formed and that AC was homogeneously loaded in the PLGA NP matrix.

3.3. FTIR

FTIR spectroscopy allowed for the identification of functional group changes not only in the curcumin and AC but also in all PLGA and LNPs, as presented in Fig. 4. The characteristic absorption peaks commonly observed from curcumin (Fig. 4A (i)) and AC (Fig. 4A (ii)) at approximately 3545, 3032, 2975, 1597, and 1283 cm^{-1} could be ascribed to the stretching frequencies of the OH, ArC—H, C—H, C═C, and C—O functional groups, respectively. However, a prominent sharp characteristic absorption band was identified for the α, β-unsaturated carbonyl peak at 1626 cm^{-1} in curcumin, and after acetylation, this peak was shifted from 1626 to 1775 cm^{-1}, which could be responsible for the formation of a new ester functional group (Fig. 4A (ii)). In addition, the broad band for the hydroxyl group of curcumin at 3545 cm^{-1} disappeared after the acetylation reaction, which clearly suggests that new acetyl groups were attached on both the hydroxyl groups that were present on the curcumin molecule. On the other hand, other than the PLGA NPs, the peak responsible for the stretching frequency of ester was observed at 1760 cm^{-1} due to the presence of AC in all samples (Fig. 4B (ii, iv, and v)); a similar peak was also found at 1740 cm^{-1} because of the polymeric ester bond that was present in PLGA NPs, as depicted in Fig. 4B (i). Notably, there was a broad band recognized at approximately 3100–3650 cm^{-1}, which was assigned to the presence of water moisture in the inner core of the LNPs (Fig. 4B (iii)), and this peak gradually decreased in ACLNPs (Fig. 4B (iv)) and ACPCSLNPs (Fig. 4B (v)) due to the fact that the inner core was occupied by AC and AC-loaded PLGA polymer matrices, respectively. Interestingly, broad bands were also observed for LNPs (Fig. 4B (iii)) at approximately 1690 to 1845 cm^{-1}, which may correspond to the presence of ester functionalities in the liposomes with inner core moisture. These peaks were significantly sharpened after the successful loading of AC into the inner cores of ACLNPs and ACPCSLNPs [59,60]. In addition, the characteristic bands at 3035, 2925, and 1085 cm^{-1} were ascribed to the stretching frequencies of ArC—H, C—H, and C—O bending vibrations, respectively. Based on the functional group analysis, AC, PLGA NPs, LNPS, ACLNPs, and ACPCSLNPs were formed successfully.

3.4. NMR

The chemical structure of AC formation from curcumin was confirmed using ^{1}H and ^{13}C NMR spectra, as depicted in Fig. 5, and notable changes were distinguished before and after acetylation. The phenolic proton of the curcumin ^{1}H NMR signal resonance was identified at δ

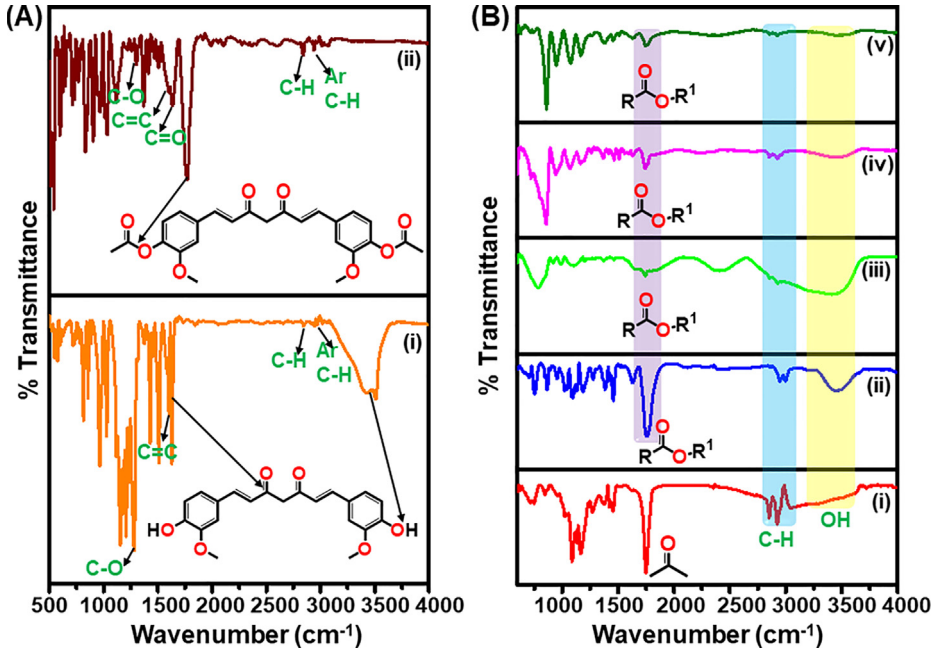

Fig. 4. FTIR spectra of (A) curcumin (i), AC (ii), and (B) PLGA NPs (i), AC loaded PLGA NPs (ii), neat LNPs (iii), ACLNPs (iv), and ACPCSLNPs (v). All FTIR spectra were recorded using KBr pellet approach, where KBr pellet acting as a transparent sheet in the infrared region.

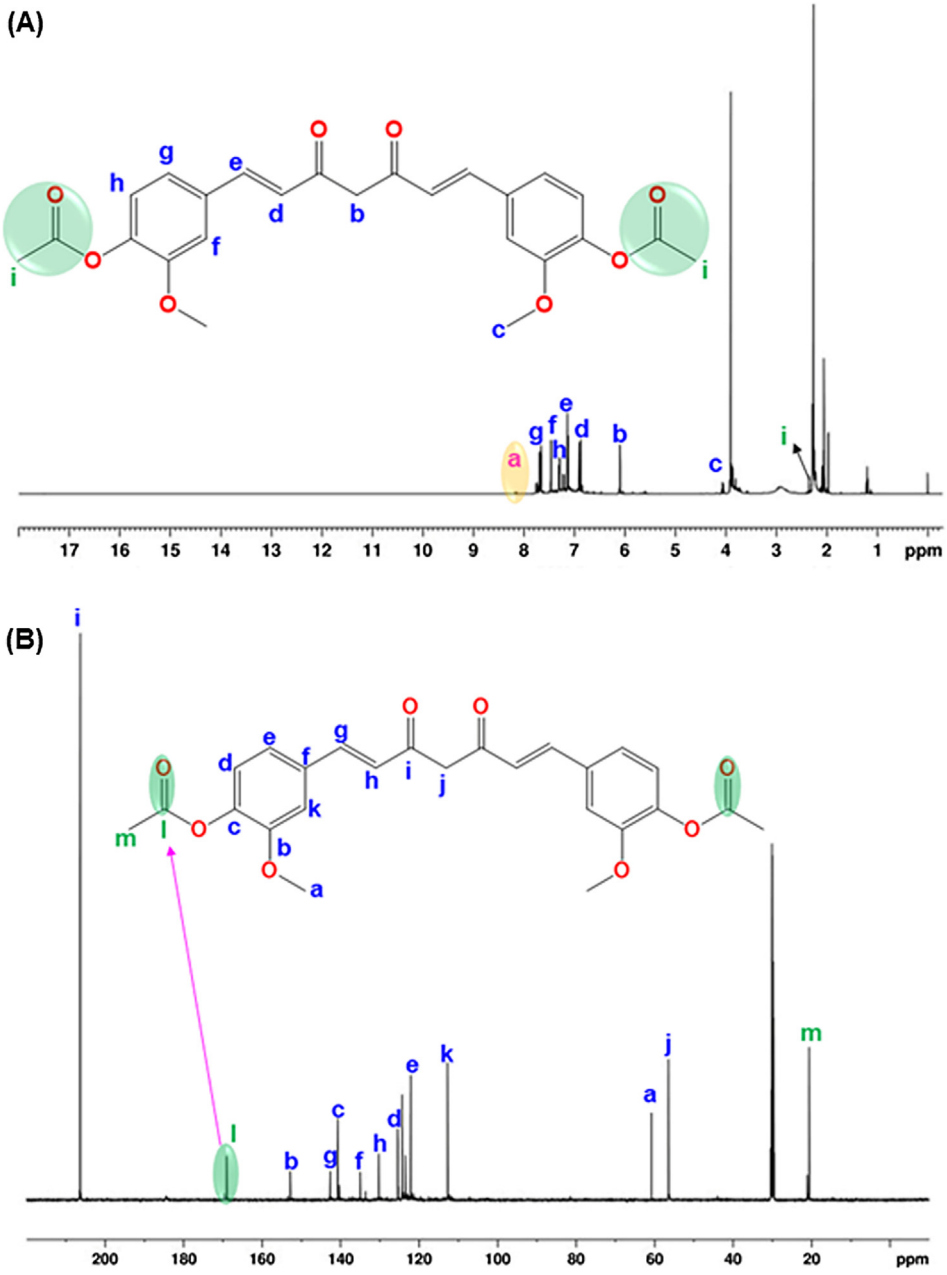

Fig. 5. (A) ^{1}H NMR and (B) ^{13}C NMR spectra of as-prepared AC. The curcumin, and AC ^{1}H and ^{13}C NMR spectra were recorded in acetone-d_6 using 500 MHz Bruker Avance III NMR instrument.

8.22 ppm (Fig. S5), and the corresponding peak disappeared after the formation of AC (Fig. 5A). In the ^{13}C NMR spectra for AC, two additional carbon peaks were recognized as resonance signals at δ 168.97 and 210.6 ppm, which could be attributed to the carbonyl group of the acetyl molecule and adjacent CH_3 (methyl) groups, respectively (Fig. 5B); in contrast, the respective ^{13}C NMR resonance signals were not detected in curcumin (Fig. S6). From the results of NMR, it could be concluded that AC was formed from curcumin by an acetylation reaction without any side products.

3.5. XPS

Additionally, XPS analysis was used to further characterization of ACPCSLNPs, and Fig. 6 represents the respective elemental composition along with the existing surface groups of ACPCSLNPs. The total XPS survey revealed the presence of three important elemental peaks at approximately 286, 399, and 533 eV, which account for the C 1s, N 1s, and O 1s, respectively (Fig. 6A). The high-resolution deconvoluted XPS spectra are presented in Fig. 6B-D. Interestingly, the high-resolution C 1s spectra can be fitted into three major peaks that are ascribed to the presence of C═C/C−C, C−N, and C═O at binding energies of 284.51, 285.92, and 288.29 eV, respectively (Fig. 6B). Fig. 6C illustrates the high resolution of the N 1s spectra and reveals the existence of only one peak at 399.41 eV, which accounted for the quaternary ammonium ions (C_4-N^+) of the choline moiety from L-α-phosphatidylcholine. The high resolution of the O 1s spectra (Fig. 6D) deconvoluted into two peaks at binding energies of 531.08 and 532.29 eV, which were attributed to C−O−C/C−OR and C═O, respectively. The presence of the C═C peak from the C 1s XPS spectra ensured that the as-prepared ACPCSLNPs were loaded with AC, and the C═O peak was comprised of the carbonyl peak of the lipid moiety and AC [61].

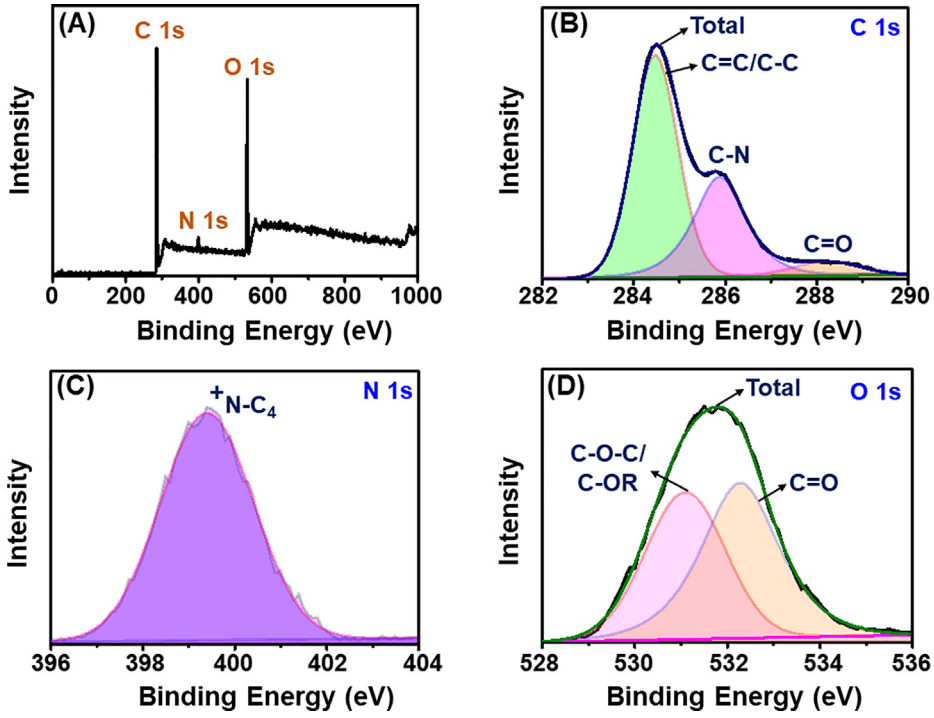

Fig. 6. XPS spectrum of the ACPCSLNPs, (A) total survey, high-resolution XPS spectra of (B) C 1s, (C) N 1s, and (D) O 1s.

3.6. Optical properties

A detailed investigation was performed using UV–vis and PL spectra analysis before and after treatment with AC and curcumin. Fig. S10 shows the absorption spectra for AC and curcumin in ethanol (Fig. S10A) and PBS at pH 7.4 (Fig. S10B), and it can be concluded that distinguishable changes were noted before and after acetylation. However, both spectra represented the UV–vis spectra of curcumin and showed a prominent absorption peak at 428 nm in the overall characteristic absorption range of approximately 300–500 nm, which is responsible for the extended π-conjugation of π - π* along with a weak absorption peak at 250–290 (curve i). Notably, a blueshift occurred in the absorption spectra from 428 to 397 nm after acetylation (curve ii). Furthermore, the UV peak was also broadened in PBS after acetylation along with a blueshift, which may be attributed to the interaction of AC with phosphate ions and the respective solvent. In addition, the photographic color changes before (left inset) and after reaction (right inset) are presented in Fig. S10A and B for curcumin and AC and show bright yellow and light yellow colors, respectively. Furthermore, we also recorded the PL spectra for AC and curcumin in ethanol (Fig. S11A) and PBS (Fig. S11B) at pH 7.4 because of their tremendous fluorescent properties. Interestingly, both compounds exhibited different emission properties under the same excitation conditions in ethanol and PBS, and a prominent blueshift was also observed, similar to that in the UV–vis absorption spectra. However, curcumin (Fig. S11, (line i)) showed a characteristic PL λ_{Emi} at 540 nm when it was excited at 388 nm, and after treatment, the λ_{Emi} peak was shifted from 540 to 465 nm under the same excitation conditions, as illustrated in Fig. S11A, (line ii). Similarly, significant PL peak emissions were also observed at 560 and 470 nm for curcumin (Fig. S11B, (line i)) and AC (Fig. S11B, (line ii)), respectively, along with blueshifts when they were excited at 388 nm. The corresponding photographic images were also presented in the inset, and curcumin (left inset) and AC (right inset) were yellow and bluish green in color in both solvents, respectively. Based on these findings, AC was successfully formed after reacting curcumin with acetic anhydride. UV–vis absorption spectra were also recorded for PLGA NPs, LNPs, ACLNPs, and ACPCSLNPs, as depicted in Fig. S13. The PLGA NPs showed (curve i) an absorption band at 270 nm, which may correspond to the presence of n-π* transitions of the carbonyl functional group in the PLGA polymer. Notably, a small peak was also identified in LNPs (curve iv) at 290 nm, which was also attributed to the presence of the n-π* transition of the carbonyl functional group of the ester moiety in L-α-phosphatidylcholine. As explained earlier, AC has two characteristic absorption peaks at 428 and 270 nm (curve ii). However, owing to the presence of a characteristic absorption peak at 428 nm due to the presence of an extended π -π* conjugation in PLGA NPs (curve iii), LNPs (curve v), and PCSLNPs (curve vi), these nanoparticles were confirmed to be successfully loaded with the active drug AC.

3.7. Kinetic study for the analysis drug release profiles

The drug release profiles with kinetic parameters were investigated in three cases including the drug-loaded (curcumin and AC) LNPs, core/shell LNPs, and PLGA NPs at neutral pH (pH = 7.4) and at pH 5.2. The reason for studying the drug release profile at pH 5.2 is to explore the acidic carcinogenic environment pool. Fig. S14 represents the UV–vis absorption spectra for different concentrations of AC at pH 7.4 (Fig. S14A), and the corresponding calibration curve of AC over different concentration ranges from 1 to 180 μM (since we loaded 8.1 mg of drug, which is equivalent to 180 μM) showed a good linear relationship with a correlation coefficient of 0.9945. The entire study for drug release profile analyses was established using the calibration plot presented in Fig. S14B. Based on Table S1 in the SI, the as-developed DDS showed significant drug release profiles over a long period of approximately 96 h (4 days) before reaching a saturation point, and the saturation point was achieved by the solubility of AC in PBS solution. First, it is evident from the analysis that there was an initial burst of drug release within ~11 and ~15 h for curcumin (Fig. S15A) and AC (Fig. S15B), respectively, from the LNPs in both pH conditions, followed by a gradual increase up to ~75 and ~65% of the total release amount after 96 h. In addition, the released drug profiles have been fitted into the power law equation, which was derived by the Korsmeyer-Peppas (K-P) model, to evaluate the proper prediction of drug release kinetics and

mechanisms using the below expression [62–64]:

$$\frac{Q_t}{Q_\infty} = k_R t^n \quad (2)$$

where Q_t/Q_∞ is the amount of drug released at time t, k_R is the relaxation constant, and n is the release exponent. As per the K-P model, n = 0.43 is equated to Fickian diffusion, 0.43 < n < 0.89 corresponds to non-Fickian transport, n = 0.85 is classified as Case II transport, and n > 0.859 corresponds to Super Case II transport for a 3D spherical matrix [65]. According to the figure, the data were not completely fitted into the K-P model because of the high fraction of drug release. Thus, the data were curve fit by the K-P model with the following two convenient adjustable parameters: one between 0 and 10 h (magnified Figure i) and the second from 15 to 96 h (magnified Figure ii). The fitted released exponents were k_R = 48.86, n = 0.64, and k_R = 44.01, n = 0.68 for CLNPs at pH 5.2 and 7.4, respectively, while for AC, the released exponents were k_R = 32.34, n = 0.93, and k_R = 27.91, n = 1.09 for ACLNPs at pH 5.2 and 7.4, respectively. As per the K-P model analysis, all fitted exponents were greater than 0.43, which indicates that the release kinetics fit classical non-Fickian transport and deviates from the Case II and Super Case II transport systems for CLNPs and ACLNPs, respectively (Table S1 in SI).

Additionally, we investigated the drug release profiles with K-P model-fitted kinetic parameters from drug-loaded (curcumin/AC) PCSLNPs, as illustrated in Fig. 7. Interestingly, the amount of drug released was dramatically decreased when using PCSLNP compared to using the neat LNPs due to the presence of the inner PLGA polymer matrix. However, initial burst releases were recognized as curcumin (Fig. 7A) and AC (Fig. 7B) within ~15 and 11 h, followed by a slow release of drug that almost leveled off after a long period (96 h), as depicted in Fig. 7. The relevant data were also curve fitted by the K-P model with two adjustable parameters, as seen in the magnified Figure i and ii. The obtained n values were greater than 0.85, which indicated that both of the DDS, CPCSLNPs and ACPCSLNPs, deviated the non-Fickian transport and Super Case II systems, respectively (Table S1). Finally, the cumulative drug release profile of PLGA NPs that were synthesized via an electrospray system and its corresponding kinetic fit models were represented in Fig. S16. Unlike the drug release profile of LNPs and PCSLNPs, the profile of PLGA NPs followed a linear response, which was well-predicted by a simplified Higuchi model.

The Higuchi model predicts the profile by using the cumulative percentage of released drug versus square root of time as explained below [66,67]:

$$\frac{Q_t}{Q_\infty} = k_H t^{1/2} \quad (3)$$

where k_H is the release rate constant, and Q_t is the amount of drug released at time t. According to Fig. S16, the drug release profiles of CPLGA-NPs (Fig. S16C) and ACPLGA-NPs (Fig. S16D) were fitted to the Higuchi kinetic model as a function of square root of time, and the cumulative release indicated approximate linearity with a good fit and correlation coefficients of more than 0.995 in both cases at both pH conditions. In addition, the Higuchi model produced good compliance with the release kinetics of CPLGA-NPs with k_H values of 10.33 and 09.96 at pH 5.2 and 7.4, respectively; the k_H values were found to be 08.81 and 08.36 at pH 5.2 and 7.4, respectively, for ACPLGA-NPs (corresponding information is summarized in Table S1).

3.8. Mechanism for sustaining drug release profile

Fig. 8 shows the plausible working mechanism for drug release (curcumin/AC) from the LNPs (Fig. 8A) and PCSLNPs (Fig. 8B). The solubility, molecular interactions such as hydrogen bonding (H-bonding), van der Waal forces and drug stability play essential roles in the drug release profile. Thus, based on the solubility and molecular interactions, we have proposed a reasonable and acceptable working mechanism in this report. As explained in the earlier section, the curcumin solubility is slightly higher than that of AC in PBS solution because of the presence of hydroxyl functional groups within the molecule, which thereby enhance the solubility via intermolecular hydrogen bonding (IMHB). As a result, curcumin is more able to participate in IMHB with the polar head groups of lipid moieties, which are present inside of the liposome core, by polar bonding attractions. Eventually, more curcumin molecules are released at a faster rate compared with that of AC to the environment outside of the LNPs, as illustrated in Fig. 8A. In contrast, the acetyl groups of AC reduce the solubility of AC

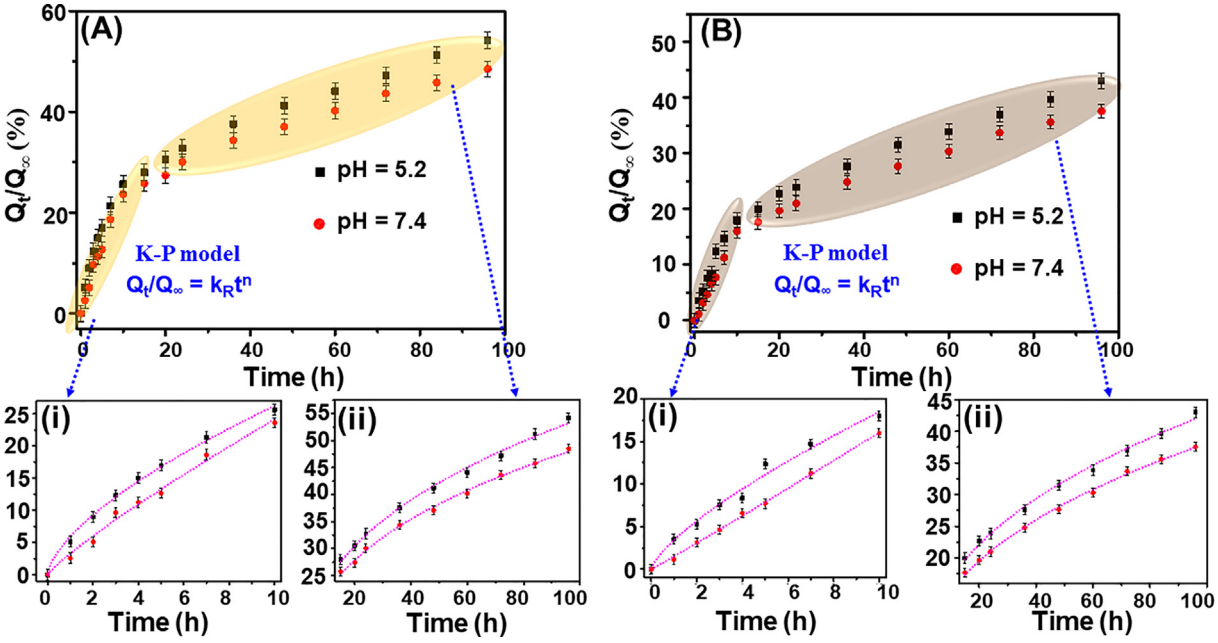

Fig. 7. The cumulative percentage of drug release profiles for curcumin (A), AC (B), and corresponding figures for the kinetic fit of models with the best two adjustable parameters (initial (magnified Figure i) and final (magnified Figure ii)) versus time from the PCSLNPs in PBS at pH 5.2 and 7.4 conditions. The data are represented as the mean ± standard deviation of three independent experiments.

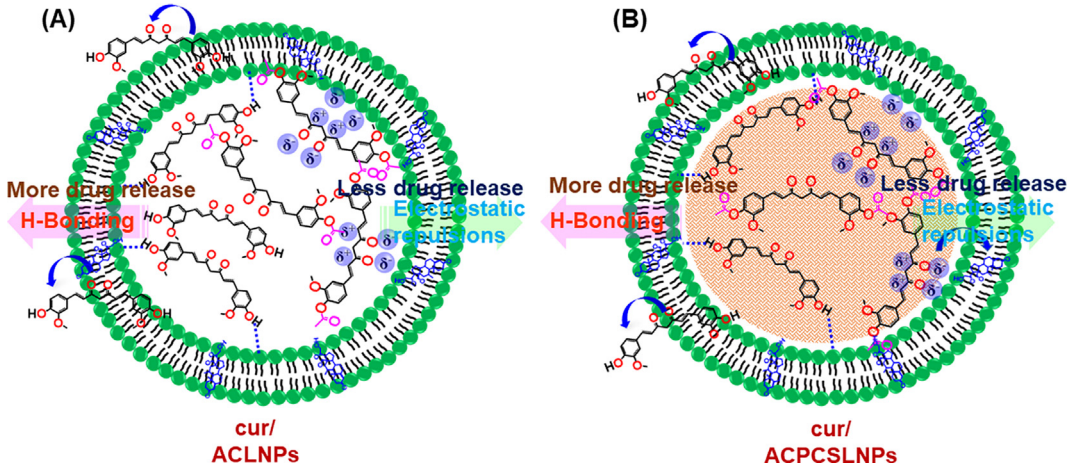

Fig. 8. Schematic illustration of the probable working mechanism of drug release (curcumin/AC) from LNPs and PCSLNPs.

to be slightly less than that of curcumin due to the absence of IMHB and the presence of electrostatic repulsions that enable the slow drug release profile. However, the mechanistic scenario of PCSLNPs is distinct when we compare it with that of the neat LNPs. In the PCSLNPs, the inner core was completely filled by the biodegradable polymer PLGA matrix. As a consequence, electrostatic interactions are generated between AC and the PLGA polymer matrix because of their solubility in organic phase solvents. After the incorporation of curcumin and AC into the PLGA polymer matrix, curcumin has the chance to release into the inner core of the liposome at a faster rate due to the presence of IMHB with the polar head groups of the lipid moieties; however, AC may not release as quickly as curcumin because of the electrostatic interactions between AC and PLGA polymer matrix (Fig. 8B).

Furthermore, it is also evident from our observations that the drug release profile was increased moderately at pH 5.2 compared to that at pH 7.4; this finding may be attributed to the enhancement of the drug molecule solubility, which eventually allows more drug release from the system [68,69]. In addition, PLGA polymeric ester bonds may also degrade more rapidly in the presence of an acidic medium, which eventually enables more drug release into the site [70]. The complete drug release profile at different pH conditions with the amount of drug released even after 96 h was illustrated in Table S1. Ultimately, the drug release profile for LNPs was identified as an initial burst followed by a final slow release, which may be due to the rapid dissolution of the drug that was present in the lipid bilayer followed by the entrapment of the drug within the core by different interactions, such as hydrogen bonding and electrostatic repulsions, respectively. Notably, based on the earlier possible reasons, the drug release profiles and corresponding data from the LNPs were fitted to the K-P model because the initial burst occurred quickly for molecules that were present in the lipid bilayer, and the subsequent slow release occurred by normal diffusion mechanisms. In contrast, the drug release profile for PLGA NPs occurred by regular diffusion and at distinct time intervals, which eventually fit into the linear curve of the Higuchi model.

3.9. Cell toxicity studies by MTT assay

An MTT [3-(4,5-dimethylthiazol-2-yl)-2,5-diphenyltetrazolium bromide] assay was employed to assess the cytotoxicity effect of liposomes (free curcumin, AC, ACLNPs and ACPCSLNPs) at different concentrations ranging from 0 to 30 μM against HeLa and HDFa cells. According to the *in vitro* studies, the cytotoxicity effects have been significantly increased upon addition of higher concentrations of samples. On the contrary, considerable cytotoxic effects were not observed (i.e., mortality of ~80%) when the samples were treated with the similar experimental conditions in HDFa cells. However, AC showing higher cytotoxicity (~31.2%) towards HeLa cells than the curcumin (~32.8%) due to presence of more absorptivity by its lipophilic nature when cells were treated at 30 μM concentration of samples for 48 h. On the other hand, ACPCSLNPs are exhibiting considerable less cytotoxic efficacies (~36.8%) than the ACLNPs (~34.2%) because of having its sustain release properties have been obtained from the lipid bilayer, and polymer moiety as well under the similar circumstances. (Fig. 9A). It can be seen from the figure that approximately 50% of the cell proliferation rate was inhibited. The results obtained from the MTT assay showed that the IC_{50} value was 20 μM for ACPCSLNPs in HeLa cells. In the same manner, Fig. 9B shows the cytotoxicity of the ACPCSLNPs against healthy fibroblast cells (HDFa), but it was determined that ACPCSLNPs had little cytotoxicity to these cells. Thus, these results indicate that the ACPCSLNPs have more dose-dependent cytotoxicity toward HeLa cell lines than to HDFa cells.

3.10. Cell viability studies by the live-dead assay

A live-dead cell staining assay was employed to assess the cytotoxic effects to HeLa and HDFa cell lines at the representative time intervals (0, 12, 24, 36 and 48 h) using ACPCSLNPs. Fig. S20 shows that the rate of dead cells in the ACPCSLNP-treated HeLa cells increased in a time-dependent manner from 0 to 48 h. However, in the ACPCSLNP-treated HDFa cells, a minimal number of dead cells was observed. The observations suggest that ACPCSLNPs have a minimal influence on healthy HDFa cells and a significant cytotoxic effect on HeLa cells. The percentage of cell viability achieved in HeLa and HDFa cell lines, when treated ACPCSLNPs were summarized in Fig. S21 and S22. For any developed drug screening, assessment of *in vitro* cell viability and cytotoxicity assays are very important to evaluate both compound toxicity and tumor cell growth inhibition. In this study, it is essential to know how many viable cells are remaining and/or how many cells are lifeless in the last part of the experiment. Here the developed ACPCSLNPs are extremely toxic to the cancerous Hela cells but significantly non-toxic to the HDFa cells.

3.11. Cancer cell imaging studies

Fluorescence microscopy was used to investigate the bio-imaging efficiency of AC (Fig. 10A), curcumin (Fig. 10B) and ACPCSLNPs (Fig. 10C) in HeLa cells. Significant fluorescence signals were observed using curcumin and AC because of their fluorescent behavior. In addition, multicolor fluorescence was observed in ACPCSLNP-treated HeLa cells, which displayed blue, green, and red emissions using excitation wavelengths of 405 nm, 488 nm, and 543 nm, respectively. Furthermore, the multicolor fluorescence behavior was responsible for the

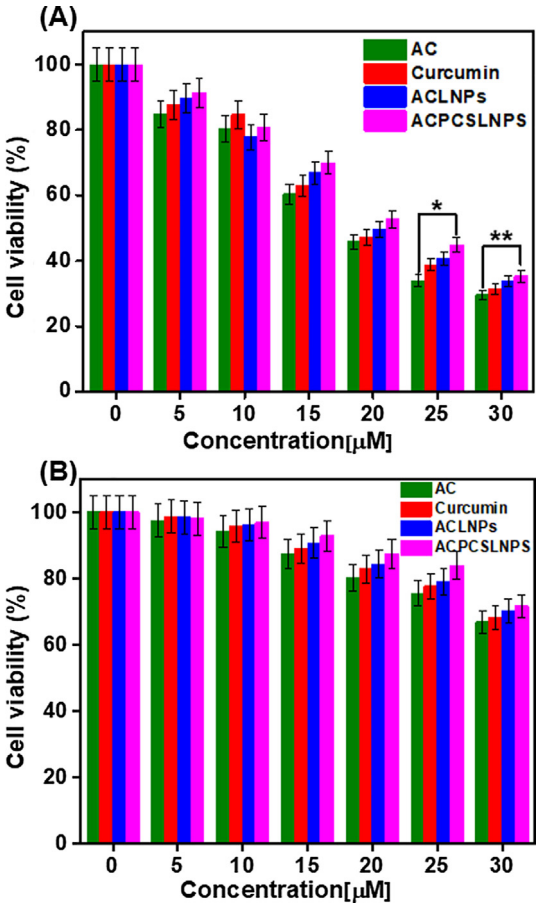

Fig. 9. MTT assay for the (A) HeLa and (B) HDFa cell lines treated with AC (green bars), curcumin (red bars), ACLNPs (blue bars) and ACPCSLNPs (pink bars). The cell viability has been performed after incubation of 48 h at 37 °C with 5% CO_2 using MTT assay. The error bars representing Mean ± SD (n = 3) *p < 0.05 and **p < 0.01. (For interpretation of the references to color in this figure legend, the reader is referred to the web version of this article.)

excitation-dependent emission properties of the ACPCSLNPs due to the presence of AC in the inner core of the liposome. The above results were well supported in the published literature [71]. These results suggest that ACPCSLNPs are well distributed in HeLa cells and can be utilized as an efficient nanomaterial for cell imaging studies.

4. Conclusions

In summary, the active drug AC was synthesized from the naturally occurring bioactive compound curcumin via an acetylation reaction. Subsequently, distinct neat and polymer-loaded core/shell liposome nanoparticles with and without AC loading were prepared using an electrospray system in the presence of an applied electric field, along with CLNPs, CPLGA-NPs and ACPLGA-NPs. The synthesized drug loaded LNPs and PLGA NPs were thoroughly characterized using various morphological, functional and analytical tools. Then, the potential sustained drug delivery mechanisms and kinetic parameters were investigated using ACLNPs and ACPCSLNPs and were compared with other nanoparticle DDS such as CLNPs, CPCSLNPs, CPLGA-NPs and ACPLGA-NPs. Interestingly, the sustained drug release profile of AC from PCSLNPs was distinct due to the presence of electrostatic interactions between AC and the PLGA polymer matrix. This system was also compared with other DDS including CLNPs and PLGA NPs. Notably, a slightly prolonged and sustained drug delivery profile was recorded over a long period of time (4 days) with a low percentage of drug release (~37%), which is equivalent to a release of ~2.4 mg out of 8.1 mg used. In addition, the drug release capability was also examined in an acidic environment (pH 5.2) along with a neutral environment (pH 7.4), and our results demonstrated that the drug release capability was slightly enhanced when the pH of the solution decreased (7.4 to 5.2) due to the formation of more hydrogen bonds, which eventually facilitates the diffusion of more drug molecules by enhancing the solubility of the drug molecules into the system. Based on these findings, the as-developed ACPCSLNPs are able to be used for any medical application as an innovative model for potential drug delivery vehicles. Interestingly, the as-synthesized ACPCSLNPs demonstrated an IC_{50} value of 20 μM in HeLa cells, but minimal cytotoxicity was observed in HDFa cells. With the obtained results from the *in vitro* cell viability and cytotoxicity assays, we conclude that the developed ACPCSLNPs are non-toxic to the HDFa cells but exhibiting significant toxic to the

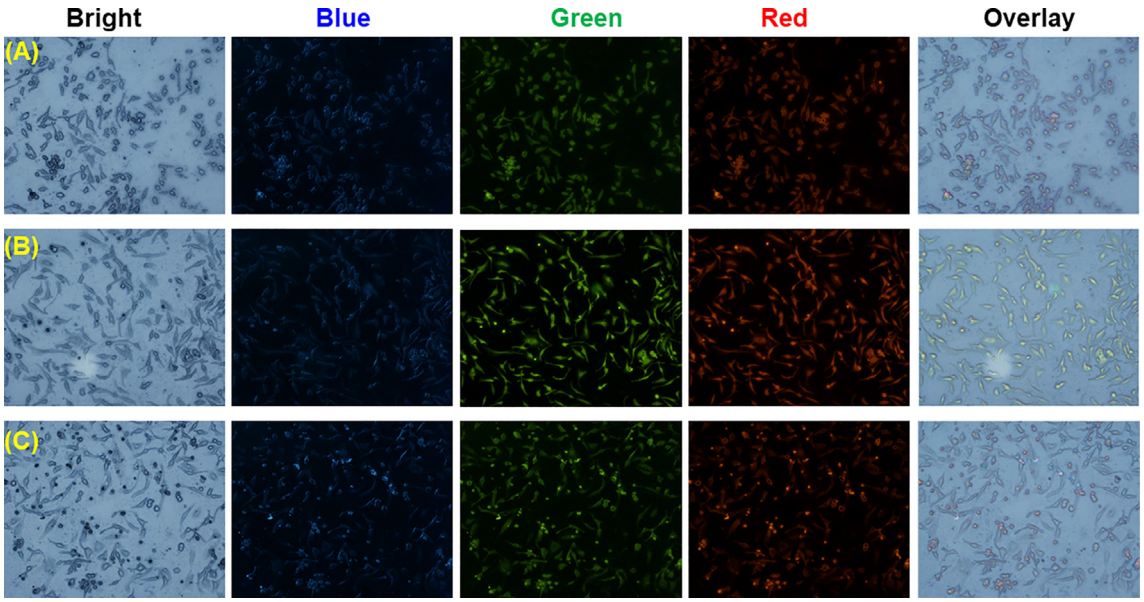

Fig. 10. Fluorescence microscopy images of HeLa cells that were treated with AC (A), curcumin (B) and ACPCSLNPs (C) under an excitation wavelength of 405 nm (blue), 488 nm (green), and 543 nm (red), as well as the overlay. The cell lines were incubated in 10% FBS and 1% antibiotics and incubated for 24 h at 37 °C with 5% CO_2 and recorded the fluorescence images. (For interpretation of the references to color in this figure legend, the reader is referred to the web version of this article.)

cancerous Hela cells. Moreover, multicolor cell imaging properties were also exhibited by ACPCSLNPs. Based on the above mentioned observations, ACPCSLNPs can be successfully employed in drug delivery, bio-imaging and anticancer studies. Furthermore, these liposomes reveal new directions for both *in vitro* and *in vivo* biomedical research with a variety of potential applications.

Declaration of Competing Interest

The authors declare no competing financial interest.

Acknowledgements

This research was supported by Basic Science Research Program through the National Research Foundation of Korea (NRF) funded by the Ministry of Education (NRF-2017R1D1A1B04035070). Human Resource Development of the Korea Institute of Energy Technology Evaluation and Planning (KETEP) and the Ministry of Trade Industry and Energy (MOTIE) of the Republic of Korea (20174030201530).

Appendix A. Supplementary material

Photographic color changes, liposome nanoparticle images, DLS, SEM, FTIR, ^{1}H and ^{13}C NMR, UV-vis spectra, PL spectra, calibration profile, kinetic models, live-dead assay results, kinetic parameters, percent of drugs released, and drug release profile tables. Supplementary data to this article can be found online at https://doi.org/10.1016/j.ejpb.2019.07.024.

References

[1] M.P. Gleeson, A. Hersey, D. Montanari, J. Overington, Probing the links between *in vitro* potency, ADMET and physicochemical parameters, Nat. Rev. Drug Discov. 10 (3) (2011) 197.
[2] Y. Henchoz, B. Bard, D. Guillarme, P.A. Carrupt, J.L. Veuthey, S. Martel, Analytical tools for the physicochemical profiling of drug candidates to predict absorption/distribution, Anal. Bioanal. Chem. 394 (3) (2009) 707–729.
[3] M.P. Stewart, R. Langer, K.F. Jensen, Intracellular delivery by membrane disruption: mechanisms, strategies, and concepts, Chem. Rev. 118 (16) (2018) 7409–7531.
[4] R.X. Zhang, T. Ahmed, L.Y. Li, J. Li, A.Z. Abbasi, X.Y. Wu, Design of nanocarriers for nanoscale drug delivery to enhance cancer treatment using hybrid polymer and lipid building blocks, Nanoscale 9 (4) (2017) 1334–1355.
[5] R. Langer, New methods of drug delivery, Science 249 (4976) (1990) 1527–1533.
[6] B. Crivelli, E. Bari, S. Perteghella, L. Catenacci, M. Sorrenti, M. Mocchi, S. Faragò, G. Tripodo, A. Prina-Mello, M.L. Torre, Silk fibroin nanoparticles for celecoxib and curcumin delivery: ROS-scavenging and anti-inflammatory activities in an in vitro model of osteoarthritis, Eur. J. Pharm. Biopharm. 137 (2019) 37–45.
[7] N. Kamaly, B. Yameen, J. Wu, O.C. Farokhzad, Degradable controlled-release polymers and polymeric nanoparticles: mechanisms of controlling drug release, Chem. Rev. 116 (4) (2016) 2602–2663.
[8] R.E. Ghitescu, A.M. Popa, A. Schipanski, C. Hirsch, G. Yazgan, V.I. Popa, R.M. Rossi, K. Maniura-Weber, G. Fortunato, Catechin loaded PLGA submicron-sized fibers reduce levels of reactive oxygen species induced by MWCNT in vitro, Eur. J. Pharm. Biopharm. 122 (2018) 78–86.
[9] K. Yang, L. Feng, Z. Liu, Stimuli responsive drug delivery systems based on nano-graphene for cancer therapy, Adv. Drug Deliv. Rev. 105 (2016) 228–241.
[10] M.N. Al-Qattan, P.K. Deb, R.K. Tekade, Molecular dynamics simulation strategies for designing carbon-nanotube-based targeted drug delivery, Drug Discov. Today 23 (2) (2018) 235–250.
[11] J. Zaloga, M. Pöttler, G. Leitinger, R.P. Friedrich, G. Almer, S. Lyer, E. Baum, R. Tietze, R. Heimke-Brinck, H. Mangge, F. Dörje, Pharmaceutical formulation of HSA hybrid coated iron oxide nanoparticles for magnetic drug targeting, Eur. J. Pharm. Biopharm. 101 (2016) 152–162.
[12] J. Liu, Z. Luo, J. Zhang, T. Luo, J. Zhou, X. Zhao, K. Cai, Hollow mesoporous silica nanoparticles facilitated drug delivery via cascade pH stimuli in tumor microenvironment for tumor therapy, Biomaterials 83 (2016) 51–65.
[13] X. Luan, K. Rahme, Z. Cong, L. Wang, Y. Zou, Y. He, H. Yang, J.D. Holmes, C.M. O'Driscoll, J. Guo, Anisamide-targeted PEGylated gold nanoparticles designed to target prostate cancer mediate: Enhanced systemic exposure of siRNA, tumour growth suppression and a synergistic therapeutic response in combination with paclitaxel in mice, Eur. J. Pharm. Biopharm. 137 (2019) 56–67.
[14] P. Horcajada, T. Chalati, C. Serre, B. Gillet, C. Sebrie, T. Baati, J.F. Eubank, D. Heurtaux, P. Clayette, C. Kreuz, J.S. Chang, Porous metal–organic-framework nanoscale carriers as a potential platform for drug delivery and imaging, Nat. Mater. 9 (2) (2010) 172.
[15] S. Hossain, E.H. Chowdhury, T. Akaike, Nanoparticles and toxicity in therapeutic delivery: the ongoing debate, Ther. Deliv. 2 (2) (2011) 125–132.
[16] G.P. van Balen, C.A. Martinet, G. Caron, G. Bouchard, M. Reist, P.A. Carrupt, R. Fruttero, A. Gasco, B. Testa, Liposome/water lipophilicity: methods, information content, and pharmaceutical applications, Med. Res. Rev. 24 (3) (2004) 299–324.
[17] D.D. Lasic, Novel applications of liposomes, Trends Biotechnol. 16 (7) (1998) 307–321.
[18] T. Olusanya, Haj R. Ahmad, D. Ibegbu, J. Smith, A. Elkordy, Liposomal drug delivery systems and anticancer drugs, Molecules 23 (4) (2018) 907.
[19] I. Sauer, I.R. Dunay, K. Weisgraber, M. Bienert, M. Dathe, Anapolipoprotein E-derived peptide mediates uptake of sterically stabilized liposomes into brain capillary endothelial cells, Biochemistry 44 (6) (2005) 2021–2029.
[20] M.A. Fontes, G.C. Vaz, T.Z. Cardoso, M.F. de Oliveira, M.J. Campagnole-Santos, R.A. dos Santos, N.M. Sharma, K.P. Patel, F. Frézard, GABA-containing liposomes: neuroscience applications and translational perspectives for targeting neurological diseases, Nanomed-Nanotechnol. 14 (3) (2018) 781–788.
[21] T. Matoba, J.I. Koga, K. Nakano, K. Egashira, H. Tsutsui, Nanoparticle-mediated drug delivery system for atherosclerotic cardiovascular disease, J. Cardiol. 70 (3) (2017) 206–211.
[22] Y.C. Barenholz, Doxil®—the first FDA-approved nano-drug: lessons learned, J. Control. Release 160 (2) (2012) 117–134.
[23] J.A. Silverman, S.R. Deitcher, Marqibo®(vincristine sulfate liposome injection) improves the pharmacokinetics and pharmacodynamics of vincristine, Cancer Chemoth. Pharm. 71 (3) (2013) 555–564.
[24] M. Mahajan, R. Kaur Khurana, N. Shri Sahajpal, P. Utreja, R. Sankar, B. Singh, S. Kumar Jain, Emerging strategies and challenges for controlled delivery of taxanes: A comprehensive review, Curr. Drug Metab. 16 (6) (2015) 453–473.
[25] N. Casagrande, M. Celegato, C. Borghese, M. Mongiat, A. Colombatti, D. Aldinucci, Preclinical activity of the liposomal cisplatin lipoplatin in ovarian cancer, Clin. Cancer Res. 20 (21) (2014) 5496–5506.
[26] A. Rodrigues, J. Matos, A. Nova Dias, B. Almeida, A. Pires, A. Pereira, J. Araújo, M.J. Queiroz, E. Castanheira, P. Coutinho, Development of multifunctional liposomes containing magnetic/plasmonic $MnFe_2O_4$/Au core/shell nanoparticles, Pharmaceutics 11 (1) (2019) 10.
[27] J. Tao, W. Fei, H. Tang, C. Li, C. Mu, H. Zheng, F. Li, Z. Zhu, Angiopep-2 conjugated "core-shell" hybrid nanovehicles for targeted and pH-triggered delivery of arsenic trioxide into glioma, Mol. Pharm. 16 (2) (2019) 786–797.
[28] K. Hadinoto, A. Sundaresan, W.S. Cheow, Lipid–polymer hybrid nanoparticles as a new generation therapeutic delivery platform: a review, Eur. J. Pharm. Biopharm. 85 (3) (2013) 427–443.
[29] G. Mikhaylov, U. Mikac, A.A. Magaeva, V.I. Itin, E.P. Naiden, I. Psakhye, L. Babes, T. Reinheckel, C. Peters, R. Zeiser, M. Bogyo, Ferri-liposomes as an MRI-visible drug-delivery system for targeting tumours and their microenvironment, Nat. Nanotechnol. 6 (9) (2011) 594.
[30] S. Krishnamurthy, R. Vaiyapuri, L. Zhang, J.M. Chan, Lipid-coated polymeric nanoparticles for cancer drug delivery, Biomater. Sci. 3 (7) (2015) 923–936.
[31] H. Wang, P. Zhao, W. Su, S. Wang, Z. Liao, R. Niu, J. Chang, PLGA/polymeric liposome for targeted drug and gene co-delivery, Biomaterials 31 (33) (2010) 8741–8748.
[32] Z. Wang, P.C. Ho, Self-assembled core-shell vascular-targeted nanocapsules for temporal antivasculature and anticancer activities, Small 6 (22) (2010) 2576–2583.
[33] C.M. Hu, S. Kaushal, H.S. Cao, S. Aryal, M. Sartor, S. Esener, M. Bouvet, L. Zhang, Half-antibody functionalized lipid− polymer hybrid nanoparticles for targeted drug delivery to carcinoembryonic antigen presenting pancreatic cancer cells, Mol. Pharm. 7 (3) (2010) 914–920.
[34] J. Gao, Y. Xia, H. Chen, Y. Yu, J. Song, W. Li, W. Qian, H. Wang, J. Dai, Y. Guo, Polymer–lipid hybrid nanoparticles conjugated with anti-EGF receptor antibody for targeted drug delivery to hepatocellular carcinoma, Nanomedicine 9 (2) (2014) 279–293.
[35] Y. Liu, K. Li, J. Pan, B. Liu, S.S. Feng, Folic acid conjugated nanoparticles of mixed lipid monolayer shell and biodegradable polymer core for targeted delivery of Docetaxel, Biomaterials 31 (2) (2010) 330–338.
[36] A. Aravind, P. Jeyamohan, R. Nair, S. Veeranarayanan, Y. Nagaoka, Y. Yoshida, T. Maekawa, D.S. Kumar, AS1411 aptamer tagged PLGA-lecithin-PEG nanoparticles for tumor cell targeting and drug delivery, Biotechnol. Bioeng. 109 (11) (2012) 2920–2931.
[37] Z. Yang, X. Luo, X. Zhang, J. Liu, Q. Jiang, Targeted delivery of 10-hydroxycamptothecin to human breast cancers by cyclic RGD-modified lipid–polymer hybrid nanoparticles, Biomed. Mater. 8 (2) (2013) 025012.
[38] X. Su, Z. Wang, L. Li, M. Zheng, C. Zheng, P. Gong, P. Zhao, Y. Ma, Q. Tao, L. Cai, Lipid-polymer nanoparticles encapsulating doxorubicin and 2′-deoxy-5-azacytidine enhance the sensitivity of cancer cells to chemical therapeutics, Mol. Pharm. 10 (5) (2013) 1901–1909.
[39] S.D. Kong, M. Sartor, C.M. Hu, W. Zhang, L. Zhang, S. Jin, Magnetic field activated lipid–polymer hybrid nanoparticles for stimuli-responsive drug release, Acta Biomater. 9 (3) (2013) 5447–5452.
[40] A.J. Mieszawska, Y. Kim, A. Gianella, I. van Rooy, B. Priem, M.P. Labarre, C. Ozcan, D.P. Cormode, A. Petrov, R. Langer, O.C. Farokhzad, Synthesis of polymer–lipid nanoparticles for image-guided delivery of dual modality therapy, Bioconjugate Chem. 24 (9) (2013) 1429–1434.
[41] M. Zheng, C. Yue, Y. Ma, P. Gong, P. Zhao, C. Zheng, Z. Sheng, P. Zhang, Z. Wang, L. Cai, Single-step assembly of DOX/ICG loaded lipid–polymer nanoparticles for highly effective chemo-photothermal combination therapy, ACS nano 7 (3) (2013) 2056–2067.
[42] R.H. Fang, C.M. Hu, K.N. Chen, B.T. Luk, C.W. Carpenter, W. Gao, S. Li, D.E. Zhang, W. Lu, L. Zhang, Lipid-insertion enables targeting functionalization of erythrocyte

membrane-cloaked nanoparticles, Nanoscale 5 (19) (2013) 8884–8888.
[43] A.J. Mieszawska, A. Gianella, D.P. Cormode, Y. Zhao, A. Meijerink, R. Langer, O.C. Farokhzad, Z.A. Fayad, W.J. Mulder, Engineering of lipid-coated PLGA nanoparticles with a tunable payload of diagnostically active nanocrystals for medical imaging, Chem. Comm. 48 (47) (2012) 5835–5837.
[44] J.A. Copp, R.H. Fang, B.T. Luk, C.M. Hu, W. Gao, K. Zhang, L. Zhang, Clearance of pathological antibodies using biomimetic nanoparticles, Proc. Natl. Acad. Sci. USA 111 (37) (2014) 13481–13486.
[45] Y. Zheng, B. Yu, W. Weecharangsan, L. Piao, M. Darby, Y. Mao, R. Koynova, X. Yang, H. Li, S. Xu, L.J. Lee, Transferrin-conjugated lipid-coated PLGA nanoparticles for targeted delivery of aromatase inhibitor 7α-APTADD to breast cancer cells, Int. J. Pharm. 390 (2) (2010) 234–241.
[46] World Health Organization. Guide to cancer early diagnosis.
[47] J. Mann, Natural products in cancer chemotherapy: past, present and future, Nat. Rev. Cancer. 2 (2) (2002) 143.
[48] P. Anand, A.B. Kunnumakkara, R.A. Newman B.B., Aggarwal Bioavailability of Curcumin: problems and promises, Mol. Pharm. 4 (6) (2007) 807–818.
[49] A.M. Fernández-Romero, F. Maestrelli, P. Mura, A. Rabasco, M. González-Rodríguez, Novel Findings about double-loaded curcumin-in-HPβcyclodextrin-in liposomes: effects on the lipid bilayer and drug release, Pharmaceutics 10 (4) (2018) 256.
[50] M. Ma, M. Lei, X. Tan, F. Tan, N. Li, Theranostic liposomes containing conjugated polymer dots and doxorubicin for bio-imaging and targeted therapeutic delivery, RSC Adv. 6 (3) (2016) 1945–1957.
[51] T. Feng, Y. Wei, R.J. Lee, L. Zhao, Liposomal curcumin and its application in cancer, Int. J. Nanomed. 12 (2017) 6027.
[52] J.A. Tapia-Hernandez, P.I. Torres-Chavez, B. Ramirez-Wong, A. Rascon-Chu, M. Plascencia-Jatomea, C.G. Barreras-Urbina, N.A. Rangel-Vazquez, F. Rodriguez-Felix, Micro-and nanoparticles by electrospray: advances and applications in foods, J. Agric. Food Chem. 63 (19) (2015) 4699–4707.
[53] J.A. Bhushani, C. Anandharamakrishnan, Electrospinning and electrospraying techniques: Potential food based applications, Trends Food Sci. Technol. 38 (1) (2014) 21–33.
[54] Z. Esmaili, S. Bayrami, F.A. Dorkoosh, H. Akbari Javar, E. Seyedjafari, S.S. Zargarian, V. Haddadi-Asl, Development and characterization of electrosprayed nanoparticles for encapsulation of Curcumin, J. Biomed. Mater. Res. A 106 (1) (2018) 285–292.
[55] B.A. Lakshmi, S. Kim, Quercetin mediated gold nanoclusters explored as a dual functional nanomaterial in anticancer and bio-imaging disciplines, Colloids Surf. B 178 (2019) 230–237.
[56] W. Deng, W. Chen, S. Clement, A. Guller, Z. Zhao, A. Engel, E.M. Goldys, Controlled gene and drug release from a liposomal delivery platform triggered by X-ray radiation, Nat. Commun. 9 (1) (2018) 2713.
[57] A. Rashidinejad, E.J. Birch, D. Sun-Waterhouse, D.W. Everett, Delivery of green tea catechin and epigallocatechin gallate in liposomes incorporated into low-fat hard cheese, Food Chem. 156 (2014) 176–183.
[58] B.S. Pattni, V.V. Chupin, V.P. Torchilin, New developments in liposomal drug delivery, Chem. Rev. 115 (19) (2015) 10938–10966.
[59] C. Bonechi, A. Donati, G. Tamasi, A. Pardini, H. Rostom, G. Leone, S. Lamponi, M. Consumi, A. Magnani, C. Rossi, Chemical characterization of liposomes containing nutraceutical compounds: Tyrosol, hydroxytyrosol and oleuropein, Biophys. Chem. 246 (2019) 25–34.
[60] X. Yi, Q. Zheng, B. Ding, M.H. Pan, Y.S. Chiou, L. Li, Z. Li, Liposome-whey protein interactions and its relation to emulsifying properties, LWT-Food Sci. Technol. 99 (2019) 505–512.
[61] Y. Zhang, A. Savva, S. Wustoni, A. Hama, I.P. Maria, A. Giovannitti, I. McCulloch, S. Inal, Visualizing the solid-liquid interface of conjugated copolymer films using fluorescent liposomes, ACS Appl. Mater. Interfaces 1 (5) (2018) 1348–1354.
[62] R.W. Korsmeyer, R. Gurny, E. Doelker, P. Buri, N.A. Peppas, Mechanisms of potassium chloride release from compressed, hydrophilic, polymeric matrices: effect of entrapped air, J. Pharm. Sci. 72 (10) (1983) 1189–1191.
[63] V.A. Tran, S.W. Lee, A prominent anchoring effect on the kinetic control of drug release from mesoporous silica nanoparticles (MSNs), J. Colloid Interface Sci. 510 (2018) 345–356.
[64] J. Siepmann, N.A. Peppas, Modeling of drug release from delivery systems based on hydroxypropyl methylcellulose (HPMC), Adv. Drug Deliv. Rev. 64 (2012) 163–174.
[65] G.H. Son, B.J. Lee, C.W. Cho, Mechanisms of drug release from advanced drug formulations such as polymeric-based drug-delivery systems and lipid nanoparticles, J. Pharm. Investig. 47 (4) (2017) 287–296.
[66] T. Higuchi, Mechanism of sustained-action medication. Theoretical analysis of rate of release of solid drugs dispersed in solid matrices, J. Pharm. Sci. 52 (52) (1963) 1145–1149.
[67] A.V. Tran, K. Shim, T.T. Thi, J.K. Kook, S.S. An, S.W. Lee, Targeted and controlled drug delivery by multifunctional mesoporous silica nanoparticles with internal fluorescent conjugates and external polydopamine and graphene oxide layers, Acta Biomater. 74 (2018) 397–413.
[68] J. Liu, B. Boonkaew, J. Arora, S.H. Mandava, M.M. Maddox, S. Chava, C. Callaghan, J. He, S. Dash, V.T. John, B.R. Lee, Comparison of sorafenib-loaded poly (lactic/glycolic) acid and DPPC liposome nanoparticles in the *in vitro* treatment of renal cell carcinoma, J. Pharm. Sci. 104 (3) (2015) 1187–1196.
[69] X. Zhang, W. Zong, H. Bi, K. Zhao, T. Fuhs, Y. Hu, W. Cheng, X. Han, Hierarchical drug release of pH-sensitive liposomes encapsulating aqueous two phase system, Eur. J. Pharm. Biopharm. 127 (2018) 177–182.
[70] S. Jabbari, A. Ghamkhari, Y. Javadzadeh, R. Salehi, S. Davaran, Doxorubicin and chrysin combination chemotherapy with novel pH-responsive poly [(lactide-co-glycolic acid)-block-methacrylic acid] nanoparticle, J. Drug Deliv. Sci. Technol. 46 (2018) 129–137.
[71] F. Du, J. Yuan, M. Zhang, J. Li, Z. Li, M. Cao, J. Chen, L. Zhang, X. Liu, A. Gong, W. Xu, Nitrogen-doped carbon dots with heterogeneous multi-layered structures, RSC Adv. 4 (71) (2014) 37536–37541.